

Emergent flat-band physics in $d^{9-\delta}$ multilayer nickelates

Frank Lechermann

Institut für Theoretische Physik III, Ruhr-Universität Bochum, D-44780 Bochum, Germany

Recent experiments have shown that the reduced multilayer rare-earth (RE) nickel oxides of form $\text{RE}_{p+1}\text{Ni}_p\text{O}_{2p+2}$ may belong to the novel family of superconducting lanthanide nickelates. Here, the correlated electronic structure of $\text{Pr}_4\text{Ni}_3\text{O}_8$ and $\text{Nd}_6\text{Ni}_5\text{O}_{12}$ is studied by means of an advanced realistic many-body framework. It is revealed that the low-energy physics of both systems is dominated by an interplay of $\text{Ni-}d_{x^2-y^2}$ and $\text{Ni-}d_{z^2}$ degrees of freedom. Whilst the $\text{Ni-}d_{x^2-y^2}$ orbitals are always highly correlated near an (orbital-selective) Mott-insulating regime, the $\text{Ni-}d_{z^2}$ orbitals give rise to intriguing non-dispersive features. At low temperature, the Pr compound still displays QP-like $\text{Ni-}d_{x^2-y^2}$ -derived states at the Fermi level, but the interacting fermiology of the Nd compound is outshined by an emergent $\text{Ni-}d_{z^2}$ -controlling flat band. These findings translate well to the previous characterization of doped infinite-layer nickelates, and hence further make the case for a mechanism of unconventional superconductivity which is distinct from the one in high- T_c cuprates.

I. INTRODUCTION

The physics of layered nickelate compounds has recently (re)gained enormous interest due to the discovery of superconductivity in Sr-doped thin films of infinite-layer NdNiO_2 ^{1,2}. The rise of a novel family of superconducting oxides has been confirmed by subsequent same findings in akin systems of PrNiO_2 ^{3,4} as well as of LaNiO_2 type^{5,6}.

In fact, the quest for superconductivity in p -layered nickelates $\text{RE}_{p+1}\text{Ni}_p\text{O}_{3p+1(,2p+2)}$ of Ruddlesden-Popper(-like) structure with rare-earth ion RE (the oxygen stoichiometry in braces marking the topotactically reduced compounds without apical O) has a rather long history⁷⁻¹⁶. It started off from investigating single-layer La_2NiO_4 , which is structurally most akin to the $\text{Cu-}d_{x^2-y^2}$ -driven high- T_c cuprate La_2CuO_4 . But in that setting, the $\text{Ni}^{2+}(3d^8)$ ion turns out orbital-wise rather different from the reference $\text{Cu}^+(3d^9)$ ion. Further layering and topotactic reduction should therefore be most effective in singling out the $\text{Ni-}d_{x^2-y^2}$ orbital in a low-energy regime for some (effective) Ni^+ setting^{8,13}. However, single crystals for the “straightforward” infinite-layer ($p \rightarrow \infty$) materials were absent until very recently¹⁷, and therefore focus consolidated on the multilayer systems with small p . And indeed, single crystals of the reduced $p = 3$ system were successfully prepared by Zhang *et al.*¹⁵. Yet superconductivity was still not detected, but then eventually the thin-film realization of hole-doped infinite-layer nickelates made the breakthrough^{1,2}. Interestingly, the optimal hole doping for the infinite-layer compounds can effectively also be realized for systems with $p \sim 5, 6$ layers^{15,18,19}. Actually, in a very recent study Pan *et al.*²⁰ reported superconductivity in the reduced $p = 5$ compound $\text{Nd}_6\text{Ni}_5\text{O}_{12}$.

This story has a further level of complexity, since the actual electronic structure and the resulting superconducting scenario of the infinite-layer nickelates might be not of straightforward cuprate kind and is still heavily debated (see e.g. Refs. 19, 21–24 for recent reviews).

Main issues are the degree of correlation strength, the role of apparent self-doping bands, and the relevance of a $\text{Ni-}d_{x^2-y^2}$ vs. a $\text{Ni-}d_{z^2}$ multi-orbital setting at low energy. Against this challenging background, we here report a comparing first-principles many-body investigation of $\text{Pr}_4\text{Ni}_3\text{O}_8$ ($p = 3$) and the recently highlighted $\text{Nd}_6\text{Ni}_5\text{O}_{12}$ ($p = 5$).

In our previous studies of infinite-layer nickelates²⁵⁻²⁸, we argued that besides local Coulomb interactions on Ni, an effective inclusion of such local interactions on the O sites is indispensable to arrive at a reliable picture of the correlated electronic structure. Based on that viewpoint, it turns out that the infinite-layer nickelate physics is dominated by the intriguing interplay between $\text{Ni-}e_g\{d_{z^2}, d_{x^2-y^2}\}$ multi-orbital degrees. While $\text{Ni-}d_{x^2-y^2}$ is orbital-selective Mott insulating and hardly doped with holes, the $\text{Ni-}d_{z^2}$ orbital eagerly collects hole carriers and shifts as a flat band in the $k_z = 1/2$ plane of the Brillouin zone across the Fermi level in the superconducting doping region. Main result of the present work is that this emergent flat band physics in front of a highly correlated $\text{Ni-}d_{x^2-y^2}$ state is indeed also relevant for $d^{9-\delta}$ multilayer nickelates, consistent with the comparable effective hole doping for superconducting infinite-layer and multilayer nickelate. Importantly, for the Pr ($p = 3$) compound, the flat band has already passed the Fermi level, dissolving into incoherent (Hund-driven) excitations. However, it is about “in resonance” with the Fermi energy for the Nd ($p = 5$) compound. This underlines the decisive role of the $\text{Ni-}d_{z^2}$ -dominated flat-band physics for the stabilization of the superconducting phase in infinite- and multilayer nickelates.

II. THEORETICAL APPROACH

To reveal the correlated electronic structure of $\text{Pr}_4\text{Ni}_3\text{O}_8$ and $\text{Nd}_6\text{Ni}_5\text{O}_{12}$, the charge self-consistent combination^{29,30} of density functional theory (DFT), dynamical mean-field theory (DMFT) and self-interaction correction (SIC) is employed³¹. The DFT part of this

DFT+sicDMFT scheme builds up on a mixed-basis pseudopotential framework³²⁻³⁴ in the local density approximation (LDA). We address the Coulomb interactions on oxygen furthermore beyond DFT within SIC on the pseudopotential level³⁵⁻³⁷. Whereas the O(2s) orbital is by default fully corrected with a weight factor $w_{2s} = 1.0$, the reasonable choice^{31,37} $w_{2p} = 0.8$ is utilized for the O(2p) orbitals. The further screening parameter α for this SIC pseudopotential is chosen also as $\alpha = 0.8$, such that the SIC inclusion on O asks for one additional parameter in the overall computational scheme. For a further discussion of the relevance of the use of SIC on O in layered nickelates we refer to Ref. 27. Finally, the Ni sites act as quantum impurity problems in multi-site realistic DMFT, with the site-resolved correlated subspace consisting of the full Ni(3d) shell, respectively. The whole scheme is converged until self-consistency in the charge density and the self-energies is reached. Note again that the SIC incorporation enters the given framework as a modified (pseudo)potential, and is not a 'fixed correction' or 'shift' on the sole DFT level.

In the following the calculational settings are described in more detail. A $11 \times 11 \times 11$ k-point mesh is utilized for $\text{Pr}_4\text{Ni}_3\text{O}_8$, and a $5 \times 5 \times 5$ one for $\text{Nd}_6\text{Ni}_5\text{O}_{12}$. The plane-wave cutoff energy is set to $E_{\text{cut}} = 13 \text{ Ry}$ and localized basis orbitals are introduced for Pr/Nd(5d), Ni(3d) as well as O(2s, 2p). The Pr/Nd(4f) states are put in the pseudopotential frozen core, since they are not decisive for the key physics of infinite-layer nickelates³⁸. The j -resolved frozen occupation of the Pr/Nd(4f) shell is chosen with small resulting moment and only scalar-relativistic effects enter the general pseudopotential generation. The role of spin-orbit effects in the overall crystal calculations is neglected. The DMFT correlated subspace on each Ni site is governed by a full Slater Hamiltonian applied to the Ni(3d) projected-local orbitals³⁹. The projection is performed on the $N(\text{O}) \times 3 + N(\text{Ni}) \times 5 + N(\text{RE})$ Kohn-Sham (KS) states above the dominant O(2s) bands, associated with O(2p), Ni(3d) and possibly relevant RE-based bands. Here, $N(\text{element})$ amounts to the element-specific number of atoms in the unit cell, e.g. four for $\text{Pr}_4\text{Ni}_3\text{O}_8$ and five for $\text{Nd}_6\text{Ni}_5\text{O}_{12}$. This choice resembles the use of one additional KS state, i.e. $6+5+1$ in infinite-layer nickelates RENiO_2 ²⁵⁻²⁸. A Hubbard $U = 10 \text{ eV}$ and a Hund exchange $J_{\text{H}} = 1 \text{ eV}$ prove reasonable for this choice of the energy window^{25,31}. The fully-localized-limit double-counting scheme⁴⁰ is applied. Continuous-time quantum Monte Carlo in hybridization expansion⁴¹ as implemented in the TRIQS code^{42,43} is used to solve the DMFT problem. Two different system temperatures, namely $T = 193 \text{ K}$ and $T = 50 \text{ K}$ are chosen to reveal relevant coherence effects. Up to $1.5 \cdot 10^9$ Monte-Carlo sweeps are performed to reach convergence. A Matsubara mesh of 1025(2049) frequencies is used to account for the higher(lower)-temperature regime. Maximum-entropy⁴⁴ and Padé⁴⁵ methods are employed for the analytical continuation from Matsubara space onto the real-frequency axis. All calculations

are conducted for a paramagnetic regime, respectively.

III. INITIAL CHARACTERIZATION OF THE $p = 3, 5$ -LAYER NICKELATES

The reduced layered nickelates of type $\text{RE}_{p+1}\text{Ni}_p\text{O}_{2p+2}$ (see Figs. 1a,c) crystallize in a tetragonal $I4/mmm$ space group and host blocks of p NiO_2 square-lattice layers separated by RE layers. These blocks of NiO_2 and RE layers are again separated by fluorite-like REO slabs, increasing the two-dimensional character of the compounds. The here studied systems $\text{Pr}_4\text{Ni}_3\text{O}_8$ and $\text{Nd}_6\text{Ni}_5\text{O}_{12}$ are chosen for the following reasons. First, the nominal average Ni(3d) occupation amounts to⁴⁶ $d^{8.67}$ for $p = 3$ and to $d^{8.80}$ for $p = 5$. Since the superconducting region of the infinite-layer nickelates nominally spans between $\sim d^{8.75-8.85}$, the $p = 5$ compound should effectively be prone to superconductivity, while the $p = 3$ compound should reside in the hole-overdoped regime. Thin films of $\text{Nd}_6\text{Ni}_5\text{O}_{12}$ have indeed been shown to exhibit superconducting properties²⁰. For the $p = 3$ case we select $\text{Pr}_4\text{Ni}_3\text{O}_8$ since it was prepared in single-crystal form^{47,48} with metallic behavior down to lowest temperatures.

The trilayer Pr compound has two symmetry-inequivalent Ni classes: the Ni1 class corresponding with the inner NiO_2 layer and the Ni2 class associated with the outer NiO_2 layer. The quintuple-layer Nd compound has three such different classes: Ni1 for inner, Ni2 for intermediate and Ni3 for outer NiO_2 layer. Lattice parameters $a = 3.935 \text{ \AA}$ and $c = 25.485 \text{ \AA}$, as well as atomic positions are here overtaken from experiment⁴⁷ for $\text{Pr}_4\text{Ni}_3\text{O}_8$. In the case of $\text{Nd}_6\text{Ni}_5\text{O}_{12}$, the experimental c -axis parameter of the thin-film study²⁰, i.e. $c = 38.8 \text{ \AA}$, and the inplane $a = 3.92 \text{ \AA}$ from NdNiO_2 ¹ are used. The atomic positions for the Nd compound are obtained via DFT structural relaxation using the generalized-gradient approximation. This results in a somewhat stronger buckling of the non- NiO_2 layers compared to the one in the Pr compound (compare Figs. 1a,c).

The DFT characterization (to be compared with previous studies^{20,46,49-52}) of both multilayer compounds is summarized in Figs. 1b,d. We choose a *fatspec* representation for the band structures. It colors the spectrum according to the orbital weight in the spectral function $A(\mathbf{k}, \omega)$ at given (\mathbf{k}, ω) point. Of course, in the DFT limit, $A(\mathbf{k}, \omega)$ reduces to the KS band structure. Note that this *fatspec* representation differs slightly from the usual 'fatband' picture, since overlaid/crossing bands and thus non-hybridized energy areas may also appear as 'mixed-orbital' character. For instance, a Ni- d_{z^2} -dominated dispersion (magenta-colored) starts in the top panel of Fig. 1b at $\sim -1 \text{ eV}$ and closes at X with energy $\sim -0.75 \text{ eV}$. It appears blue-colored inbetween, because it overlays with Ni- t_{2g} (cyan-colored) in that energy range. Surely, the truly mixed hybridization on an individual dispersion is also correctly signalled. Here, the *fatspec* representation focusses on the Ni(3d) nature of

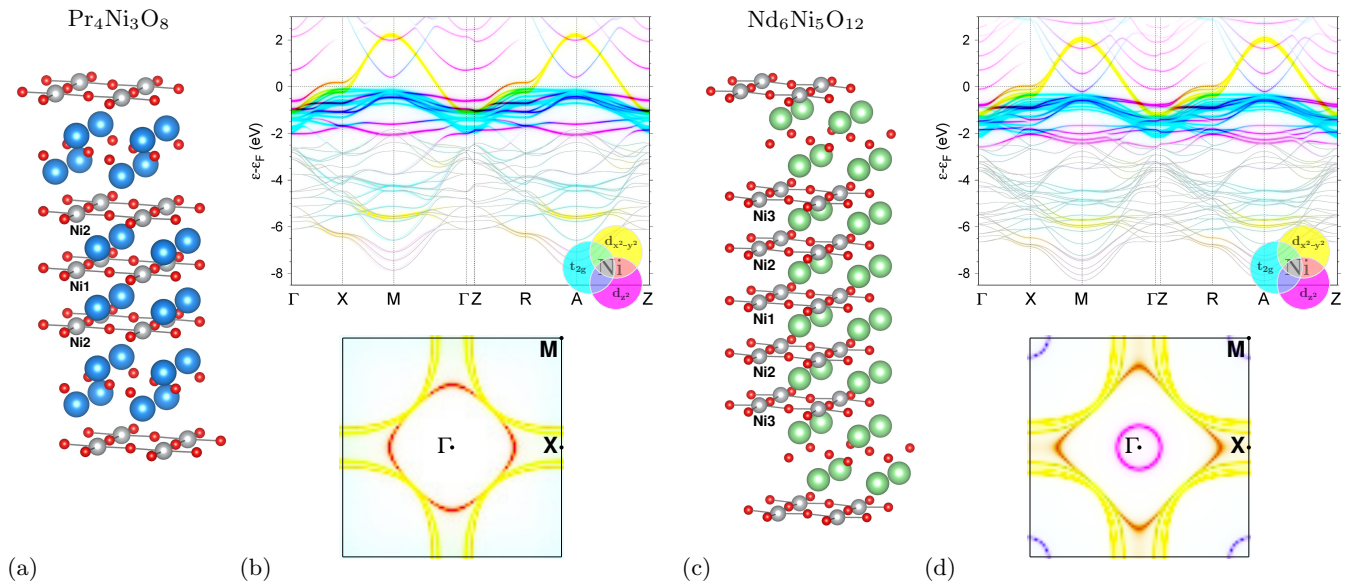


FIG. 1. (color online) Crystal structure and DFT spectrum of $\text{Pr}_4\text{Ni}_3\text{O}_8$ (a,b) and $\text{Nd}_6\text{Ni}_5\text{O}_{12}$ (c,d). (a) Structure of the $p = 3$ Pr compound with Pr (blue), Ni (grey) and oxygen (red); Ni1 and Ni2 class with associated NiO_2 layers are indicated. (b) Band structure along high-symmetry lines (top) and Fermi surface (bottom) of $\text{Pr}_4\text{Ni}_3\text{O}_8$ in Ni(3d)-fatspec (see text) representation. Note that mixed colors represent joint contributions from the involved orbitals, e.g. red color corresponds to a mixing of Ni- $d_{x^2-y^2}$ (yellow) and Ni- d_{z^2} (magenta). The O(2p)-based block of bands is drawn with full grey lines. (c) Structure of the $p = 5$ Nd compound with Nd (green), Ni (grey) and oxygen (red); Ni1, Ni2 and Ni3 class with associated NiO_2 layers are again indicated. (d) Same as (b), but for $\text{Nd}_6\text{Ni}_5\text{O}_{12}$.

the electronic structure.

Starting with $\text{Pr}_4\text{Ni}_3\text{O}_8$, it is seen that the Ni- t_{2g} -dominated bands are mostly full and only the Ni- e_g -derived bands are partially occupied. Note that there is no self-doping band as in infinite-layer nickelates²⁵, the corresponding bands with sizable Ni- d_{z^2} , Ni- t_{2g} and Pr(5d) character are well above the Fermi level ε_F . Along Γ -X, one band of mixed Ni- e_g type crosses ε_F , whilst along X-M there are two dominant Ni- $d_{x^2-y^2}$ dispersions at low-energy. In other words, there are p Ni- e_g bands crossing the Fermi level. This results in a three-sheeted Fermi surface (FS) for the Pr compound, with an electron-like mixed Ni- e_g inner sheet centred around Γ and two close-running Ni- $d_{x^2-y^2}$ -based hole-like sheets. The latter are reminiscent of the hallmark hole sheet in high- T_c cuprates.

The DFT spectrum of the Nd compound displays further-increased complexity (see Fig. 1d). Now five Ni- e_g -based bands cross ε_F ; a strongly-mixed one again along Γ -X and four along X-M. Three out of these latter four bands are dominantly of Ni- $d_{x^2-y^2}$ kind and the highest-lying one with some Ni- d_{z^2} mixed in. Note that the mixed Ni- e_g dispersion crossing in Γ -X direction has its van-Hove point at X closer to the Fermi level than in the Pr compound. Furthermore, there are two additional self-doping bands, one close to Γ and the second close to M. The first one has sizable Ni- d_{z^2} flavor, whereas the one next to M has also Ni- t_{2g} mixed in. Accordingly, besides the five-sheeted dominant Ni- e_g fermiology, the FS exhibits two additional electron-like pockets around

Γ and M. As a further difference to $\text{Pr}_4\text{Ni}_3\text{O}_8$, the most-mixed Ni- e_g sheet (i.e. red-colored in bottom panel of Figs. 1b,d) is larger and has more square shape in the Nd compound. Interestingly, the self-doping bands are seemingly missing in the $p = 5$ compound of La type^{46,52}, but are also observed in the DFT result for $\text{Nd}_6\text{Ni}_5\text{O}_{12}$ from Ref. 51.

Finally, we want to comment on the charge-transfer energy $\Delta = \varepsilon_d - \varepsilon_p$, whereby $\varepsilon_{d,p}$ are the respective band centre of Ni(3d) and O(2p). Using the DFT+sic approach, a value $\Delta_{\text{NdNiO}_2} = 5.0$ eV was obtained for infinite-layer NdNiO_2 ²⁵. For the present multilayer systems, calculations from the same perspective result in $\Delta_{\text{Nd}_6\text{Ni}_5\text{O}_{12}} = 4.2$ eV and $\Delta_{\text{Pr}_3\text{Ni}_3\text{O}_8} = 3.9$ eV. This drop of the charge-transfer energy with an increase of the Ni effective oxidation state is in line with previous findings^{28,53}.

IV. DFT+sicDMFT RESULTS

A. $\text{Pr}_4\text{Ni}_3\text{O}_8$

Let us turn to the interacting problem beyond DFT by first focussing on the trilayer Pr compound. Intuitively, from the anticipated similarity to the overdoped infinite-layer system²⁷, one may expect the correlated electronic structure of $\text{Pr}_4\text{Ni}_3\text{O}_8$ to be in a Hund(-like) regime where coherence effects and possible non-Fermi-liquid (NFL) characteristics due to an interplay of Ni- d_{z^2}

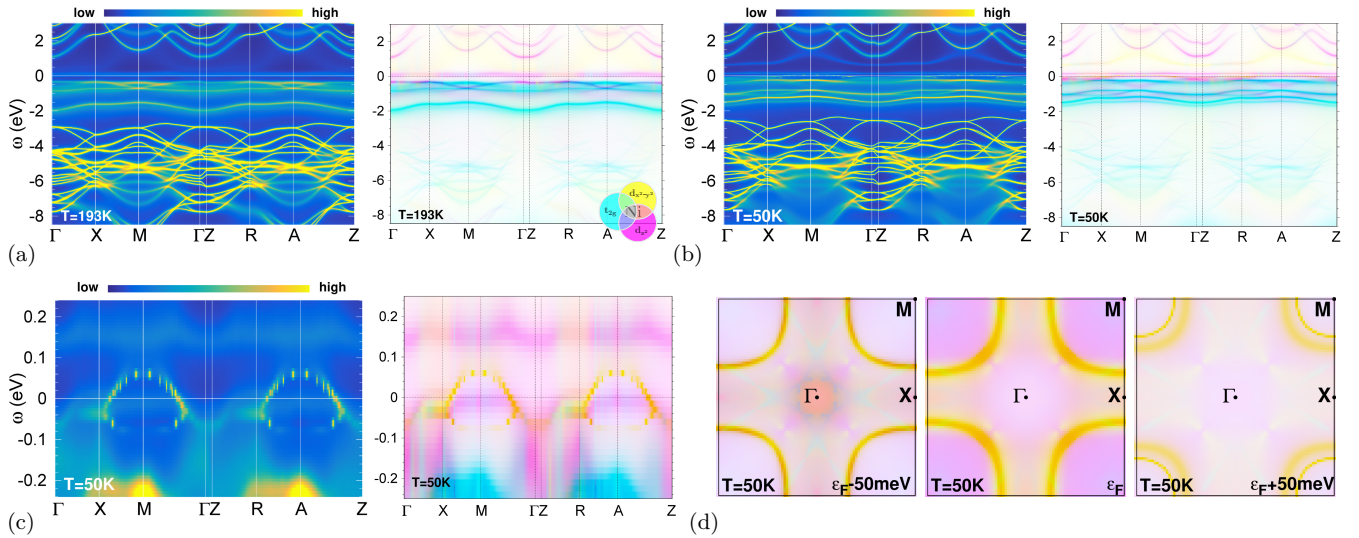


FIG. 2. (color online) \mathbf{k} -resolved DFT+sicDMFT spectrum $\text{Pr}_4\text{Ni}_3\text{O}_8$. (a) Complete $A(\mathbf{k}, \omega)$ along high-symmetry lines (left) and Ni(3d) fatspec representation (right), both at $T = 193$ K. (b) Same as (a) but at $T = 50$ K. (c) Same as (b) but focussing on low-energy window around ε_F . (d) $k_z = 0$ constant-energy surfaces at $T = 50$ K, from left to right: $\varepsilon_F - 50$ meV, ε_F , $\varepsilon_F + 50$ meV.

and Ni- $d_{x^2-y^2}$ may be important. Figure 2a shows the \mathbf{k} -resolved spectrum at $T = 193$ K ($\beta = 1/T = 60$ eV $^{-1}$), with an indeed absence of well-defined quasiparticle (QP) dispersions at the Fermi level. The Ni- $d_{x^2-y^2}$ -dominated states are very strongly correlated with large scattering rate for Ni1 and an even diverging imaginary Matsubara self-energy for Ni2 (cf. orange circle-dashed lines in right panel of Fig. 3a). The fatspec representation reveals that the Ni- t_{2g} -dominated bands remain well below ε_F . Furthermore, it displays that the near-dispersionless spectral weight at ~ 0.15 eV above the Fermi level is of Ni- d_{z^2} character. Further such character with somewhat more (incoherent) dispersion may be observed in a similar energy range below ε_F .

Lowering the temperature to $T = 50$ K leads to a significant increase of the Ni- $d_{x^2-y^2}$ coherence, resulting in highly-renormalized QP dispersions as shown in Fig. 2b,c. This Fermi-liquid (FL) regime is also observable from the associated Ni- $d_{x^2-y^2}$ self-energies for both Ni sites (cf. orange square-full lines in right panel of Fig. 3a). The effective mass $m^*/m_{\text{DFT}} \sim 14$ turns out very large for this orbital sector. In addition, notably, the impact of temperature, leading also to energy shifts for the Ni- t_{2g} -dominated bands, is stronger than in stoichiometric infinite-layer NdNiO_2 , where Ni- $d_{x^2-y^2}$ resides in an effective Mott-insulating regime throughout the accessible temperature range^{25,26}. However as seen in Fig. 2c, there is still strong incoherent Ni- d_{z^2} spectral weight at and close to the Fermi level, which adds up to an appreciable total low-energy weight upon \mathbf{k} -integration for both symmetry-inequivalent Ni sites (cf. Fig. 3b). The incoherent nature of this Ni- d_{z^2} weight is also drawn from the displayed imaginary part of the corresponding self-energies in Fig. 3a (cf. magenta square-full lines in left

panel): for Ni1 it shows a clear NFL upturn at small Matsubara frequencies, and for Ni2 the bending in the same frequency range is too strong to account for the linear-frequency behavior of a FL. In other words, the electronic regime that one encounters in $\text{Pr}_4\text{Ni}_3\text{O}_8$ is that of an partly incoherent metal with still highly-renormalized Ni- $d_{x^2-y^2}$ QP(-like) dispersions. Concerning the aforementioned connection of effective Ni charge states, this finding matches with a principal Hund-metal identification of the overdoped infinite-layer regime²⁷.

The total spectral function $A(\omega)$ (see top panel of Fig. 3b), besides the metallic weight at ε_F , shows a dominant Ni(3d) peak at ~ -0.5 eV and a dominant broader O(2p) peak at ~ -4.5 eV. Those dominant d and p peaks are shifted towards the Fermi level compared to stoichiometric NdNiO_2 , again understandable from the doping connection. Note that there is also some non-minor Pr(5d) weight located within the broader O(2p)-dominated peak, associated with the Pr sites in the fluorite-like REO slab. The Zhang-Rice character⁵⁴ of the low-energy spectral weight, i.e. a spectral sharing between Ni(3d) and O(2p), is small; the latter weight is dominantly of Ni(3d) type. In view of the Ni1, Ni2 differentiation, the inner Ni1 site exhibits a somewhat stronger Ni- $d_{x^2-y^2}$ low-energy peak structure than the outer Ni2 site. But this weight is of pseudogap structure for both sites, possibly due to the coupling to the NFL-behaving Ni- d_{z^2} states.

Table I provides the Ni(3d) fillings, and while the values for Ni- $d_{x^2-y^2}$ are always close to half filling, the Ni- d_{z^2} orbitals are mainly controlling the hole content. For $\text{Pr}_4\text{Ni}_3\text{O}_8$, the filling $n(d_{z^2})$ is lowest with an average value ~ 1.45 and some larger filling for the outer Ni2 site (translating to a slight overall larger $n(3d)$ filling for Ni2).

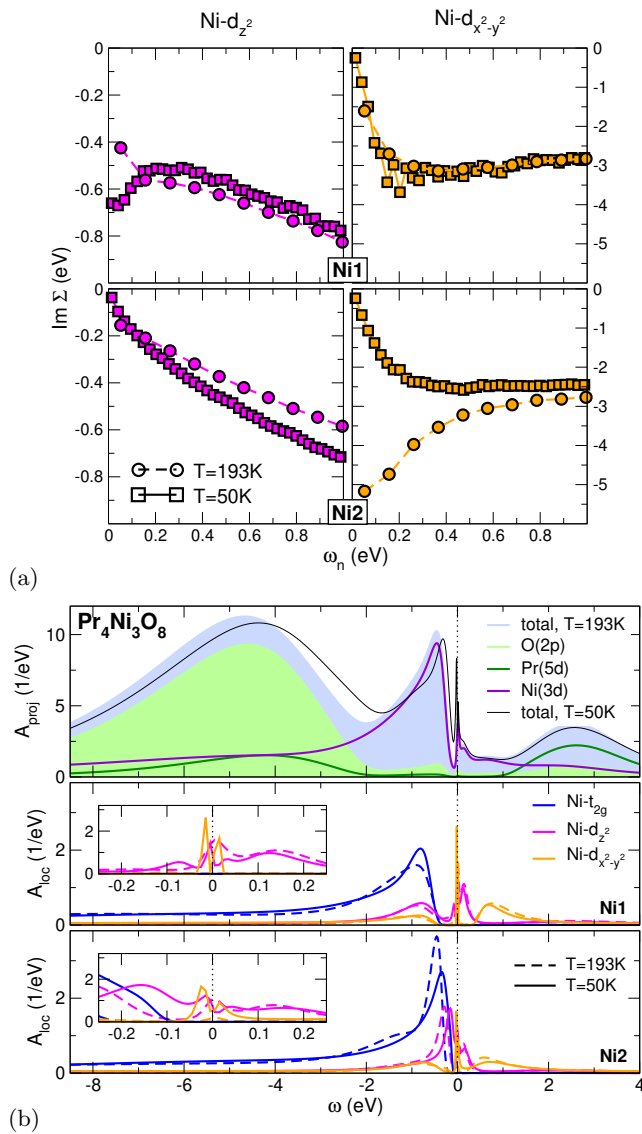


FIG. 3. (color online) Ni- e_g self-energies (a) and \mathbf{k} -integrated DFT+sicDMFT spectrum (b) of $\text{Pr}_4\text{Ni}_3\text{O}_8$. (a) Imaginary part of the Ni- d_{z^2} (left) and the Ni- $d_{x^2-y^2}$ (right) Mat-subara self-energy $\Sigma(i\omega_n)$ for Ni1 (top) and Ni2 (bottom) at $T = 193$ K (circle-dashed) and $T = 50$ K (square-full). (b) Top: total as well as element- and site-resolved projected spectral function; middle and bottom: local Ni1($3d$) and Ni2($3d$) spectral function at $T = 193$ K (dashed) and $T = 50$ K (full), respectively. Insets: low-energy window.

Albeit far off from a formal Ni^{12+} , Ni^{2+} dichotomy⁵⁵, the larger Ni($3d$) charge on Ni2 is qualitatively in line with this simple picturing. Note that the theoretical filling values from DFT+sicDMFT, as usual depending on e.g. the given definition of the correlated subspace, are generally somewhat smaller than from the simplistic aforementioned oxidation-state analysis for $p = 3, 5$. From a direct theory comparison to calculations for hole-overdoped $\text{Nd}_{1-x}\text{Sr}_x\text{NiO}_2$ with $x = 0.3$, the present $n(d_{z^2})$ for the trilayer compound is also significantly lower. Thus the

compound	Ni site	$n(d_{z^2})$	$n(d_{x^2-y^2})$	$n(3d)$
$\text{Pr}_4\text{Ni}_3\text{O}_8$	Ni1	1.40	1.13	8.47
	Ni2	1.48	1.11	8.53
$\text{Nd}_6\text{Ni}_5\text{O}_{12}$	Ni1	1.65	1.08	8.67
	Ni2	1.54	1.09	8.57
	Ni3	1.56	1.08	8.58
NdNiO_2 [27]	Ni	1.85	1.07	8.86
$\text{Nd}_{0.85}\text{Sr}_{0.15}\text{NiO}_2$ [27]	Ni	1.76	1.04	8.74
$\text{Nd}_{0.70}\text{Sr}_{0.30}\text{NiO}_2$ [27]	Ni	1.60	1.08	8.58

TABLE I. Site and orbital-resolved Ni($3d$) fillings n in the $p = 3, 5$ -layer compounds from DFT+sicDMFT at $T = 50$ K. The Ni- t_{2g} filling varies only marginally and is always close to $n(t_{2g}) = 5.94$. The comparing data²⁷ for stoichiometric and hole-doped infinite-layer NdNiO_2 was obtained for $T = 30$ K.

comparison between multilayer and doped-infinite-layer physics has still to be performed with caution.

Let us finally compare to experiment. Zhang *et al.*⁴⁷ reported metallic behavior down to lowest T , with however a rather high room-temperature resistivity of $67.2 \Omega \text{cm}$. Additionally, the specific-heat measurements from that work give rise to a large $\gamma \sim 75 \text{ mJ mol}^{-1} \text{K}^{-2}$. In comparison, for $\text{La}_4\text{Ni}_3\text{O}_8$ a value $\gamma \sim 15 \text{ mJ mol}^{-1} \text{K}^{-2}$ is obtained⁵⁶ and a mass enhancement of about 3-4 inferred. Disregarding possible Pr($4f$) physics, an enormous formal mass enhancement of ~ 15 for $\text{Pr}_4\text{Ni}_3\text{O}_8$ is thus not completely out of range. Magnetic properties have been measured by Huangfu *et al.*⁵⁷ showing complex magnetic behavior without ordering down to lowest T . But the data hints to a coexistence of localized spins and itinerant degrees of freedom.

B. $\text{Nd}_6\text{Ni}_5\text{O}_{12}$

Very much in parallel to the discussion of the correlated electronic structure of $\text{Pr}_4\text{Ni}_3\text{O}_8$ in the last section, the focus is henceforth on the $p = 5$ Nd compound. Figure. 4 displays the \mathbf{k} -resolved data, with obvious low-energy differences to the trilayer Pr system. The seemingly non-dispersive spectral weight just above the Fermi level for the latter compound, appears here more or less right at ε_F for both investigated temperatures (cf. Fig. 4a,b). At $T = 193$ K, this Fermi-level spectral weight is again very incoherent, and the Ni- $d_{x^2-y^2}$ self-energies are (about to) diverging at low frequency (see Fig. 5a). In the low-energy window of Fig. 4c for $T = 50$ K, there is some strongly renormalized Ni- $d_{x^2-y^2}$ dispersion identifiable, but its intensity seems reduced compared to the one in $\text{Pr}_4\text{Ni}_3\text{O}_8$. Instead, the non-dispersive Ni- d_{z^2} weight right at ε_F turns out stronger for the present quintuple-layer Nd compound.

Note that the self-doping bands forming electron pockets around Γ and M in the previous DFT picture are shifted well-above the Fermi level and do not play a role in the fermiology. Compared to infinite-layer NdNiO_2 ,

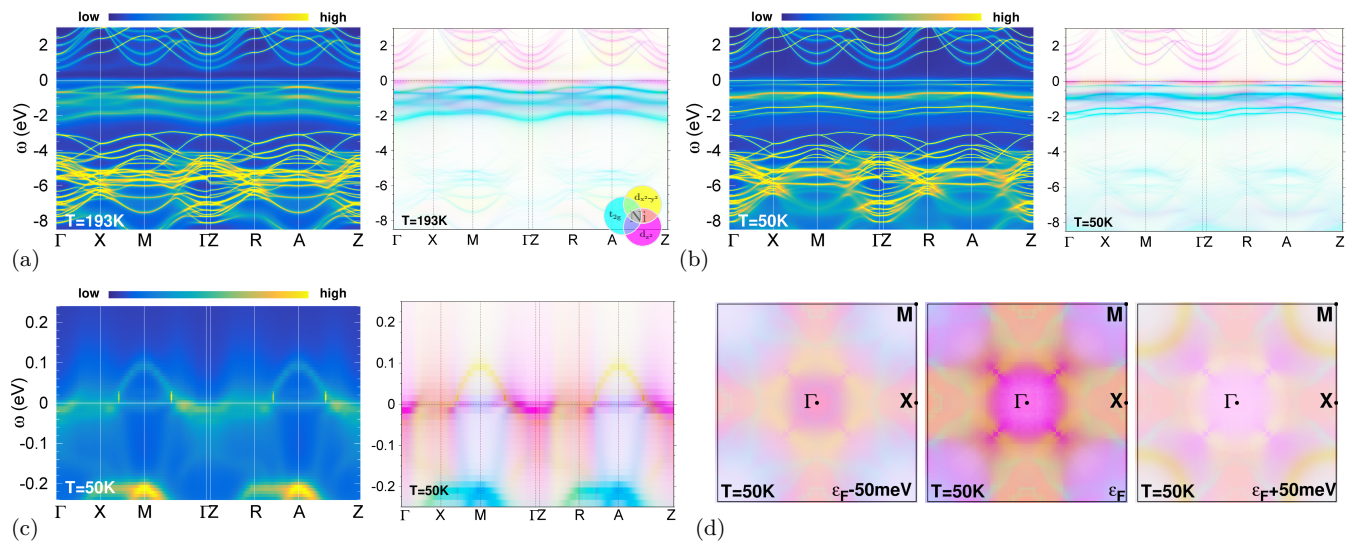


FIG. 4. (color online) Same as Fig. 2 but for $\text{Nd}_6\text{Ni}_5\text{O}_{12}$.

where the self-doping band 'survives' correlation effects and remains at the stoichiometric Fermi level, this is understandable for two main reasons. First the charge-transfer from $\text{Pr}(5d)$ to $\text{Ni}(3d)$ in order to realize a favorable (near) half-filled $\text{Ni}-d_{x^2-y^2}$ scenario in a strong-coupling limit is apparently larger for $p = 5$. Second, the self-doping bands carry quite some $\text{Ni}-d_{z^2}$ weight in both cases, however importantly, in the quintuple-layer compound the filling $n(d_{z^2})$ is way smaller than in NdNiO_2 (cf. Tab. I). Therefore, correlations in $\text{Ni}-d_{z^2}$ are stronger, enabling a larger correlation-induced shifting of the corresponding spectral weight. As for the trilayer system, the $\text{Ni}-t_{2g}$ -dominated states are mostly full. Yet there is a residual $\text{Ni}-d_{z^2}/t_{2g}$ hybridization visible in the fatspec-representation panel of Fig. 4c, extending towards the Fermi level.

Finally, the fermiology at $T = 50\text{K}$ looks quite different from the one of $\text{Pr}_4\text{Ni}_3\text{O}_8$ and rather intriguing (see Fig. 4d). The role of the previously dominant $\text{Ni}-d_{x^2-y^2}$ states is hard to decipher, but much weaker (to say the least). The original hole-like topology from this orbital sector becomes only well tractable somewhat above the Fermi level close to the M point. Apparently, the coherence scale for (possibly) robust QP-like $\text{Ni}-d_{x^2-y^2}$ excitations has not yet been reached at $T = 50\text{K}$ for $\text{Nd}_6\text{Ni}_5\text{O}_{12}$. Also therefore, mass-enhancement estimates are not too well-defined in this case. Yet from a crude examination of the low-frequency Ni self-energy, the m^* is about the twice the value than for the trilayer Pr compound. The interacting Fermi surface appears to be dominated by a correlated flat-band $\text{Ni}-d_{z^2}$ sheet around Γ . Further conclusive FS details are hard to draw from the generally low-coherence level at this temperature. Lowering the temperature much further is however numerically tough for the given theoretical approach to these multilayer systems. But still, the present results for

the two T scales render the fact robust, that emergent flat-band physics of $\text{Ni}-d_{z^2}$ type rules the low-energy response. From a site-averaged view onto the $\text{Ni}-d_{z^2}$ self-energies shown in the left panel of Fig. 5a, the correlation effects on this flat band seem somewhat weaker than for the similarly non-dispersive parts in the Pr compound. There are no very strong irregular features, however the low-frequency bending for the Ni3 site is still NFL-like.

The \mathbf{k} -integrated spectra plotted in Fig. 5b are for the total content similar to the $\text{Pr}_4\text{Ni}_3\text{O}_8$ case, with a somewhat stronger low-energy peak at ε_F and slightly deeper-energy location of the $\text{Ni}(3d)$ and $\text{O}(2p)$ peaks. The Zhang-Rice nature of the low-energy weight remains minor. The site-resolved Ni spectra exhibit seemingly a monotonic $\text{Ni}-e_g$ evolution at low energy, in the sense that the $\text{Ni}-d_{z^2}$ character grows from inner-to-outer layer and vice versa for $\text{Ni}-d_{x^2-y^2}$ (with similar pseudogap structure as for the trilayer compound). The emergent flat-band physics appears to be dominantly driven from the outer Ni3 site. Interestingly, the $\text{Ni}(3d)$ charge hierarchy between inner and outer layers turn out reversed in $\text{Nd}_6\text{Ni}_5\text{O}_{12}$; the inner Ni1 site has a slightly higher d count than Ni2, Ni3 by about 0.1 electrons (see Tab. I).

Comparison to experiment is even more difficult in the quintuple-layer case. First, there is so far only the thin-film work by Pan *et al.*²⁰ on this system. Second, even for $T = 50\text{K}$, the theoretical spectrum/fermiology has not yet completely settled in terms of coherence. The measured room-temperature resistivity of $\sim 6\text{m}\Omega\text{cm}$ yet is way smaller than for single-crystal $\text{Pr}_4\text{Ni}_3\text{O}_8$, which could be in favor of a high density of states at ε_F . The experimental Hall coefficient is positive over the whole accessible T range. A negative sign of this coefficient for stoichiometric NdNiO_2 is understandable from the self-doping electron pockets, and indeed, such pockets are missing in the interacting regime of the present multilayer

V. DISCUSSION

The revealed data for the paramagnetic correlated electronic structure of $\text{Pr}_4\text{Ni}_3\text{O}_8$ and $\text{Nd}_6\text{Ni}_5\text{O}_{12}$ shows that the two compounds share certain similarities, but possess a rather different low-energy nature. Similar to both systems is the way higher susceptibility to temperature effects than for the stoichiometric NdNiO_2 compound. Akin to the infinite-layer nickelate is the orbital-selective scenario of a highly correlated, (near) Mott-insulating $\text{Ni-}d_{x^2-y^2}$ orbital sector and an itinerant $\text{Ni-}d_{z^2}$ sector. However while the latter is close to complete filling and only weakly-correlated in stoichiometric NdNiO_2 , the correlation effects are here more severe due to a lower filling with stronger overall $\text{Ni-}e_g$ inter-orbital processes. These processes are apparently based on a sophisticated interplay between orbital-selectivity, Hund-driven mechanisms and flat-band physics within the two-orbital $\text{Ni-}e_g$ manifold. The very details of this interplay have to be addressed in a tailored model-Hamiltonian study and are not subject of the present investigation. But as result thereof, due to a different doping scenario, the trilayer Pr compound still displays $\text{Ni-}d_{x^2-y^2}$ QP(-like) excitations within a background of non-dispersive incoherent $\text{Ni-}d_{z^2}$ states, whereas $\text{Nd}_6\text{Ni}_5\text{O}_{12}$ exhibits a more incoherent $\text{Ni-}d_{x^2-y^2}$ dispersion coexisting with $\text{Ni-}d_{z^2}$ flat-band features.

Trying to rationalize this behavior, let us first focus on the $\text{Ni-}d_{x^2-y^2}$ part. From DFT+*sic*DMFT calculations for NdNiO_2 ^{25–27}, we learned that $\text{Ni-}d_{x^2-y^2}$ is effectively Mott-localized at stoichiometry and remains incoherent upon hole doping until a specific regime within the superconducting doping region. In the infinite-layer overdoped region it becomes again incoherent. Thus the $\text{Ni-}d_{x^2-y^2}$ electrons behave very differently compared to the Zhang-Rice-bound carriers in high- T_c cuprates, where coherent QPs (modulo the hallmark pseudogap regime) are robust over a wide doping ranging starting just beyond stoichiometry. The strong charge-transfer character of

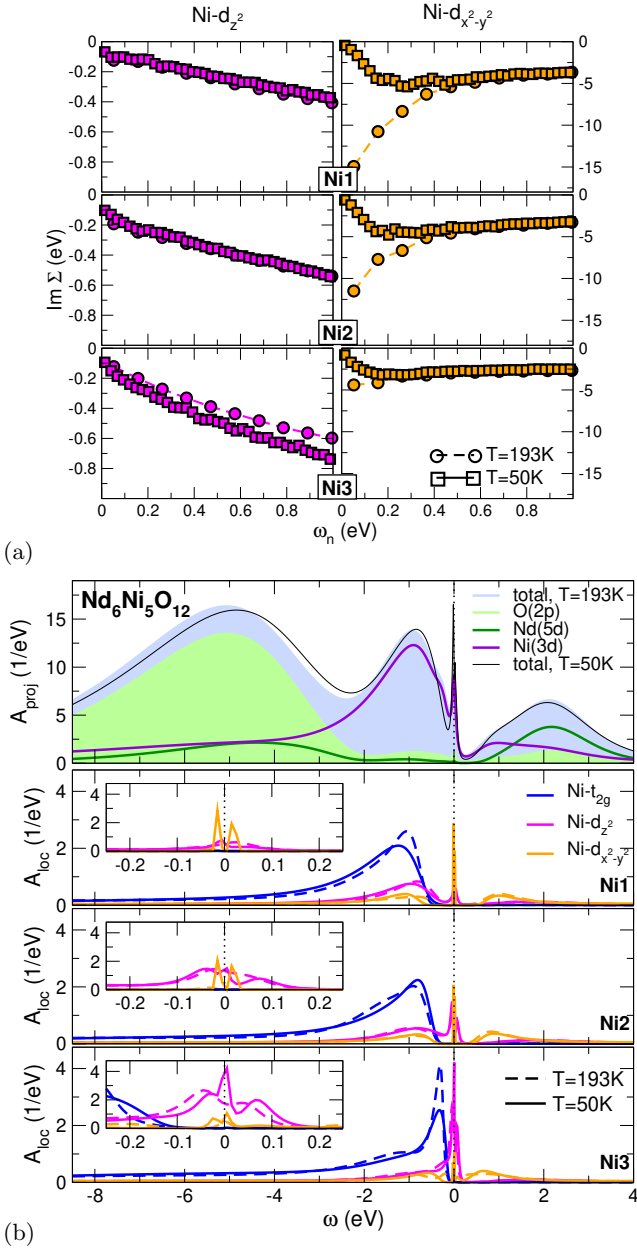


FIG. 5. (color online) Same as Fig. 3 but for $\text{Nd}_6\text{Ni}_5\text{O}_{12}$. The Ni site-resolved data spans here over Ni1, Ni2 and Ni3.

compounds. But the very intriguing (incoherent) fermiology shown in Fig. 4d does not really allow for more serious conclusions on this issue. At least, many-body calculations⁵⁸ of the Hall coefficient for optimally-doped infinite-layer NdNiO_2 results also in a positive sign when having a previously-predicted²⁵ $\text{Ni-}d_{z^2}$ flat-band at the Fermi level.

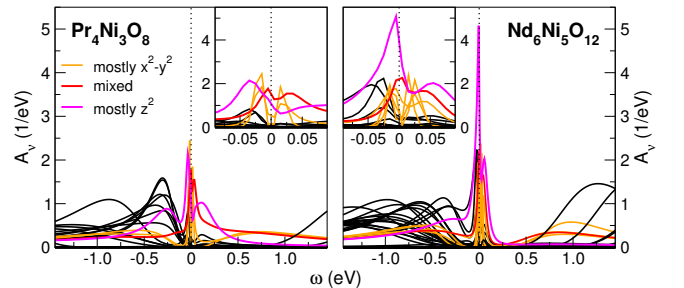


FIG. 6. (color online) Emergent flat-band character from the band-resolved correlated spectral function $A_\nu(\omega)$ (see text). Left: $\text{Pr}_4\text{Ni}_3\text{O}_8$ and right: $\text{Nd}_6\text{Ni}_5\text{O}_{12}$. Inset: focus around the Fermi level. The non-black colored functions denote the ν -resolved ϵ_F -crossing spectral weight with strongest near- $\omega = 0$ contribution. Note that the coloring in terms of $\text{Ni-}d_{z^2}$ and $\text{Ni-}d_{x^2-y^2}$ marks only dominance and is for illustration, since this not a fatspec/band plot.

these cuprates, lacking in present nickelates, appears to be main origin for this. But then it is still surprising that $\text{Pr}_4\text{Ni}_3\text{O}_8$ shows QP(-like) physics in this nominally overdoped regime from the infinite-layer perspective. Reason could be that a strong similarity between trilayer and infinite layer just breaks down in the overdoped region. For instance, the additional degree of freedom of Ni-site differentiation might allow for electronic relaxation such as to render QP propagation more robust. Another aspect may be the fact that the lanthanide neighboring compounds $\text{La}_4\text{Ni}_3\text{O}_8$ and $\text{Nd}_4\text{Ni}_3\text{O}_8$ are experimentally identified insulating at low temperature^{15,59} (though the trilayer Nd compound may be metallic in thin-film geometry²⁰). Thus the competition between metal and insulator is seemingly tight, and a QP-based metallicity of the Pr compound may also be based on subtleties that are outside the general rule.

Concerning the $\text{Ni-}d_{z^2}$ part, the difference between the 'non-dispersive' dispersion just above the Fermi level in the trilayer Pr compound and the 'flat band' right at ε_F in the quintuple-layer Nd compound has to be understood. Key is the observation that as in doped NdNiO_2 a flat band (there in the $k_z = 1/2$ plane because of a missing layer differentiation) shifts through the Fermi surface with growing hole content. This is illustrated in Fig. 6, where the band-resolved correlated spectral function $A_\nu(\omega)$ is plotted. The function $A_\nu(\omega)$ results from unfolding the local DMFT Green's function to the original crystal Hilbert space, i.e. displays how strong each original KS band is dressed with correlations and contributes to the total interacting spectrum. The red/magenta-highlighted A_ν mark the strongest non-Mott-critical contributions to the Fermi spectral weight. In the case of $\text{Pr}_4\text{Ni}_3\text{O}_8$ (left pane of Fig. 6), there are two such contributions, whereby especially the magenta-colored one still shows sizable sign of correlation (i.e. sideband features). The non-dispersive part at ~ 0.15 eV above the Fermi level in Fig. 2c may be identified with the upper sideband of that latter A_ν , peaking just a bit below ε_F . The sideband energy scale is too small for an ordinary upper Hubbard band, so a Hund-mediated origin is likely. Note that hence only two of the three original KS bands that cross the Fermi level are nearly Mott-insulating (cf. inset, orange-colored lines in Fig. 6). To make contact to the original DFT band structure (see Fig 1b): the here red-colored A_ν connects to the highest Fermi-level KS band with mixed $\text{Ni-}d_{z^2}/\text{Ni-}d_{x^2-y^2}$ character; the here magenta-colored A_ν connects to the highest-occupied KS $\text{Ni-}d_{z^2}$ -dominated dispersion, starting at ~ -1 eV at Γ and closing at ~ -0.75 eV at X. Hence intriguingly, a KS-occupied band is partly depleted in the interacting regime and causes the non-dispersive sideband feature in DFT+sicDMFT.

On the other hand for the $\text{Nd}_6\text{Ni}_5\text{O}_{12}$ compound, it is easily observed in the right panel of Fig. 6 that there is one certain A_ν of strong $\text{Ni-}d_{z^2}$ nature dominating right at the Fermi level. It is again connected to the original-KS $\text{Ni-}d_{z^2}$ -dominated dispersion just below the

$\text{Ni-}d_{x^2-y^2}$ -dominated bands (cf. Fig 1d), and describes the *emergent flat band* at ε_F . Hence in both multilayer cases, the $\text{Ni-}d_{z^2}$ dispersions below the $\text{Ni-}d_{x^2-y^2}$ -dominated ones are an important key to the problem. However it only evolves into an emergent flat band in the quintuple-layer case. In the trilayer case, since at a nominal higher hole-doping level, the formerly flat-band part of the $\text{Ni-}d_{z^2}$ dispersion has already crossed the Fermi level and dissolves into stronger (Hund-)correlated states with incoherent spectral weight. Note that as a further difference, the topmost mixed $\text{Ni-}d_{z^2}/\text{Ni-}d_{x^2-y^2}$ dispersion (red color in Fig. 6) is stronger correlated in the Nd compound.

Let us finally note, that recent DFT+DMFT studies on multilayer nickelates⁵⁰⁻⁵² differ from the here established low-energy picture. From those works, $\text{Ni-}d_{z^2}$ -influenced physics is mainly negligible and moderately-to-strongly correlated $\text{Ni-}d_{x^2-y^2}$ physics (yet distant from an obvious Mott-critical regime) is dominating. Key difference lies in the neglect of oxygen-based correlations in Refs. 50-52, which renders the layered nickelates (much) weaker correlated than described here. Future experiments have to decide which correlation regime and low-energy picture is more fitting. Note in that respect, that a recent photoemission study⁶⁰ for stoichiometric thin-films of infinite-layer PrNiO_2 reports an electronic spectrum in very good accordance with the DFT+sicDMFT predicted^{25,27} spectrum for NdNiO_2 .

VI. CONCLUSION

The present DFT+sicDMFT study predicts emergent flat-band character of $\text{Ni-}d_{z^2}$ type in the quintuple-layer nickelate $\text{Nd}_6\text{Ni}_5\text{O}_{12}$. It is due to the formation of near Mott-insulating $\text{Ni-}d_{x^2-y^2}$ states in an orbital-selective manner within the $\text{Ni-}e_g$ subshell, in conjunction with the effective (optimal) hole doping compared to stoichiometric infinite-layer NdNiO_2 . Multiorbital correlations of seemingly Hund-driven kind are also observable, but those are stronger for the trilayer nickelate $\text{Pr}_4\text{Ni}_3\text{O}_8$. The latter compound is in a nominal hole-overdoped regime compared to NdNiO_2 , however still displays as QP-like $\text{Ni-}d_{x^2-y^2}$ -dominated fermiology. Whilst the principal mapping between doped infinite-layer and multilayer nickelates exists as envisioned, some caution has to be taken concerning the details. Still in the end, the present results for the $p = 3, 5$ multilayers are consistent with our previous results on infinite-layer nickelates²⁵⁻²⁸: the eventually arising superconductivity should be unconventional in a non-cuprate manner, with the $\text{Ni-}e_g$ interplay, and especially the $\text{Ni-}d_{z^2}$ flat-band physics at the Fermi level, as a key driving force.

ACKNOWLEDGMENTS

The author thanks D. S. Dessau, A. Hampel, P. Hao, J. Karp, H. Li and A. J. Millis for helpful discussions. Support from the European XFEL and the Center for Computational Quantum Physics of the Flatiron Institute under the Simons Award ID 825141 is acknowl-

edged. The work is furthermore partially supported by the German Research Foundation within the bilateral NSFC-DFG Project ER 463/14-1. Computations were performed at the JUWELS Cluster of the Jülich Supercomputing Centre (JSC) under project numbers hhh08 and miqs.

-
- ¹ D. Li, K. Lee, B. Y. Wang, M. Osada, S. Crossley, H. R. Lee, Y. Cui, Y. Hikita, and H. Hwang, *Nature* **572**, 624 (2019).
- ² S. Zeng, C. S. Tang, X. Yin, C. Li, M. Li, Z. Huang, J. Hu, W. Liu, G. J. Omar, H. Jani, Z. S. Lim, K. Han, D. Wan, P. Yang, S. J. Pennycook, A. T. S. Wee, and A. Ariando, *Phys. Rev. Lett.* **125**, 147003 (2020).
- ³ M. Osada, B. Y. Wang, B. H. Goodge, K. Lee, H. Yoon, K. Sakuma, D. Li, M. Miura, L. F. Kourkoutis, and H. Y. Hwang, *Nano Letters* **20**, 5735 (2020).
- ⁴ M. Osada, B. Y. Wang, K. Lee, D. Li, and H. Y. Hwang, *Phys. Rev. Materials* **4**, 121801 (2020).
- ⁵ M. Osada, B. Y. Wang, B. H. Goodge, S. P. Harvey, K. Lee, D. Li, L. F. Kourkoutis, and H. Y. Hwang, arXiv:2105.13494 (2021).
- ⁶ S. W. Zeng, C. J. Li, L. E. Chow, Y. Cao, Z. T. Zhang, C. S. Tang, X. M. Yin, Z. S. Lim, J. X. Hu, P. Yang, and A. Ariando, arXiv:2105.13492 (2021).
- ⁷ M. Crespín, P. Levitz, and L. Gatineau, *J. Chem. Soc., Faraday Trans. 2* **79**, 1181 (1983).
- ⁸ P. Lacorre, *J. Solid State Chem.* **96**, 495 (1992).
- ⁹ J. Choynet, R. A. Evarestov, I. I. Tupitsyn, and V. A. Veryazov, *J. Phys. Chem. Solids* **57**, 1839 (1996).
- ¹⁰ M. A. Hayward, M. A. Green, M. J. Rosseinsky, and J. Sloan, *J. Am. Chem. Soc.* **121**, 8843 (1999).
- ¹¹ V. I. Anisimov, D. Bukhvalov, and T. M. Rice, *Phys. Rev. B* **59**, 7901 (1999).
- ¹² K.-W. Lee and W. E. Pickett, *Phys. Rev. B* **70**, 165109 (2004).
- ¹³ V. V. Poltavets, K. A. Lokshin, S. Dikmen, M. Croft, T. Egami, and M. Greenblatt, *J. Am. Chem. Soc.* **128**, 9050 (2006).
- ¹⁴ V. Pardo and W. E. Pickett, *Phys. Rev. Lett.* **105**, 266402 (2010).
- ¹⁵ J. Zhang, Y.-S. Chen, D. Phelan, H. Zheng, M. R. Norman, and J. F. Mitchell, *PNAS* **113**, 8945 (2016).
- ¹⁶ A. S. Botana, V. Pardo, W. E. Pickett, and M. R. Norman, *Phys. Rev. B* **94**, 081105 (2016).
- ¹⁷ P. Puphal, Y.-M. Wu, K. Fürsich, H. Lee, M. Pakdaman, J. A. N. Bruin, J. Nuss, Y. E. Suyolcu, P. A. van Aken, B. Keimer, M. Isobe, and M. Hepting, *Science Advances* **7**, eabl8091 (2021).
- ¹⁸ Z. Li, W. Guo, T. T. Zhang, J. H. Song, T. Y. Gao, Z. B. Gu, and Y. F. Nie, *APL Materials* **8**, 091112 (2020).
- ¹⁹ J. F. Mitchell, *Frontiers in Physics* **9**, 753 (2021).
- ²⁰ G. A. Pan, D. F. Segedin, H. LaBollita, Q. Song, E. M. Nica, B. H. Goodge, A. T. Pierce, S. Doyle, S. Novakov, D. C. Carrizales, A. T. N'Diaye, P. Shafer, H. Paik, J. T. Heron, J. A. Mason, A. Yacoby, L. F. Kourkoutis, O. Erten, C. M. Brooks, A. S. Botana, and J. A. Mundy, *Nat. Mater.* **s41563-021-01142-9** (2021).
- ²¹ A. S. Botana, F. Bernardini, and A. Cano, *JETP* **159**, 711 (2021).
- ²² J. Zhang and X. Tao, *CrystEngComm* **23**, 3249 (2021).
- ²³ W. E. Pickett, *Nat Rev Phys* **3**, 7 (2021).
- ²⁴ H. Chen, A. Hampel, J. Karp, F. Lechermann, and A. Millis, arXiv:2201.02852 (2022).
- ²⁵ F. Lechermann, *Phys. Rev. B* **101**, 081110((R)) (2020).
- ²⁶ F. Lechermann, *Phys. Rev. X* **10**, 041002 (2020).
- ²⁷ F. Lechermann, *Phys. Rev. Materials* **5**, 044803 (2021).
- ²⁸ F. Lechermann, arXiv:2111.12473 (2021).
- ²⁹ S. Y. Savrasov, G. Kotliar, and E. Abrahams, *Nature* **410**, 793 (2001).
- ³⁰ D. Grieger, C. Piefke, O. E. Peil, and F. Lechermann, *Phys. Rev. B* **86**, 155121 (2012).
- ³¹ F. Lechermann, W. Körner, D. F. Urban, and C. Elsässer, *Phys. Rev. B* **100**, 115125 (2019).
- ³² C. Elsässer, N. Takeuchi, K. M. Ho, C. T. Chan, P. Braun, and M. Fähnle, *J. Phys.: Condens. Matter* **2**, 4371 (1990).
- ³³ F. Lechermann, F. Welsch, C. Elsässer, C. Ederer, M. Fähnle, J. M. Sanchez, and B. Meyer, *Phys. Rev. B* **65**, 132104 (2002).
- ³⁴ B. Meyer, C. Elsässer, F. Lechermann, and M. Fähnle, *FORTRAN 90 Program for Mixed-Basis-Pseudopotential Calculations for Crystals*, Max-Planck-Institut für Metallforschung, Stuttgart (1998).
- ³⁵ D. Vogel, P. Krüger, and J. Pollmann, *Phys. Rev. B* **54**, 5495 (1996).
- ³⁶ A. Filippetti and N. A. Spaldin, *Phys. Rev. B* **67**, 125109 (2003).
- ³⁷ W. Körner and C. Elsässer, *Phys. Rev. B* **81**, 085324 (2010).
- ³⁸ G.-M. Zhang, Y.-F. Yang, and F.-C. Zhang, *Phys. Rev. B* **101**, 020501(R) (2020).
- ³⁹ B. Amadon, F. Lechermann, A. Georges, F. Jollet, T. O. Wehling, and A. I. Lichtenstein, *Phys. Rev. B* **77**, 205112 (2008).
- ⁴⁰ V. I. Anisimov, I. V. Solovyev, M. A. Korotin, M. T. Czyżyk, and G. A. Sawatzky, *Phys. Rev. B* **48**, 16929 (1993).
- ⁴¹ P. Werner, A. Comanac, L. de' Medici, M. Troyer, and A. J. Millis, *Phys. Rev. Lett.* **97**, 076405 (2006).
- ⁴² O. Parcollet, M. Ferrero, T. Ayrál, H. Hafermann, I. Krivenko, L. Messio, and P. Seth, *Comput. Phys. Commun.* **196**, 398 (2015).
- ⁴³ P. Seth, I. Krivenko, M. Ferrero, and O. Parcollet, *Comput. Phys. Commun.* **200**, 274 (2016).
- ⁴⁴ M. Jarrell and J. E. Gubernatis, *Physics Reports* **269**, 133 (1996).
- ⁴⁵ H. J. Vidberg and J. W. Serene, *J Low Temp Phys* **29**, 179 (1977).
- ⁴⁶ H. LaBollita and A. S. Botana, *Phys. Rev. B* **104**, 035148 (2021).

- ⁴⁷ J. Zhang, A. Botana, J. Freeland, D. Phelan, H. Zheng, V. Pardo, M. Norman, and J. F. Mitchell, *Nat. Phys.* **13**, 864 (2017).
- ⁴⁸ J. Q. Lin, P. Villar Arribi, G. Fabbris, A. S. Botana, D. Meyers, H. Miao, Y. Shen, D. G. Mazzone, J. Feng, S. G. Chiuzbăian, A. Nag, A. C. Walters, M. García-Fernández, K.-J. Zhou, J. Pellicciari, I. Jarrige, J. W. Freeland, J. Zhang, J. F. Mitchell, V. Bisogni, X. Liu, M. R. Norman, and M. P. M. Dean, *Phys. Rev. Lett.* **126**, 087001 (2021).
- ⁴⁹ E. M. Nica, J. Krishna, R. Yu, Q. Si, A. S. Botana, and O. Erten, *Phys. Rev. B* **102**, 020504 (2020).
- ⁵⁰ J. Karp, A. Hampel, M. Zingl, A. S. Botana, H. Park, M. R. Norman, and A. J. Millis, *Phys. Rev. B* **102**, 245130 (2020).
- ⁵¹ P. Worm, L. Si, M. Kitatani, R. Arita, J. M. Tomczak, and K. Held, *arXiv:2111.12697* (2021).
- ⁵² H. LaBollita and A. S. Botana, *arXiv:2111.14739* (2021).
- ⁵³ A. E. Bocquet, T. Saitoh, T. Mizokawa, and A. Fujimori, *Solid State Commun.* **83**, 11 (1992).
- ⁵⁴ F. C. Zhang and T. M. Rice, *Phys. Rev. B* **37**, 3759(R) (1988).
- ⁵⁵ M. H. Upton, J. Zhang, H. Zheng, A. Said, and J. F. Mitchell, *Journal of Physics: Condensed Matter* **32**, 425503 (2020).
- ⁵⁶ D. Rout, S. R. Mudi, M. Hoffmann, S. Spachmann, R. Klingeler, and S. Singh, *Phys. Rev. B* **102**, 195144 (2020).
- ⁵⁷ S. Huangfu, Z. Guguchia, D. Cheptiakov, X. Zhang, H. Luetkens, D. J. Gawryluk, T. Shang, F. O. von Rohr, and A. Schilling, *Phys. Rev. B* **102**, 054423 (2020).
- ⁵⁸ F. Petocchi, V. Christiansson, F. Nilsson, F. Aryasetiawan, and P. Werner, *Phys. Rev. X* **10**, 041047 (2020).
- ⁵⁹ Q. Li, C. He, X. Zhu, J. Si, X. Fan, and H.-H. Wen, *Sci. China Phys. Mech. Astron.* **64**, 227411 (2021).
- ⁶⁰ Z. Chen, M. Osada, D. Li, E. M. Been, S.-D. Chen, M. Hashimoto, D. Lu, S.-K. Mo, K. Lee, B. Y. Wang, F. Rodolakis, J. L. McChesney, C. Jia, B. Moritz, T. P. Devereaux, H. Y. Hwang, and Z.-X. Shen, *arXiv:2106.03963* (2021).